Molecular dynamics study on structure and properties of liquid and amorphous Al_2O_3

Vo Van Hoang*
Dept. of Physics, College of Nat. Sci., National Univ. of HoChiMinh City, 227 Nguyen Van Cu Str., Distr. 5, HCM City, Vietnam
(Received 17 September 2003; revised manuscript received 15 July 2004; published 15 October 2004)

Structure and thermodynamics properties of liquid and amorphous Al_2O_3 have been investigated by Static Relaxation (SR) and Molecular Dynamics (MD) methods. Simulations were done in the basic cube under periodic boundary conditions containing 3000 ions with Born-Mayer type pair potentials. Structure of liquid and amorphous Al_2O_3 models is in good agreement with experiment. The microstructure of Al_2O_3 system has been analyzed through pair radial distribution functions, coordination number distributions, interatomic distances or pore distribution (for amorphous state only). Temperature dependence of the pore distribution in amorphous Al_2O_3 was obtained. A thermal expansion coefficient and self-diffusion constants have been calculated. The temperature dependence of diffusion constants D in liquid Al_2O_3 shows an Arrhenius law with activation energies which are close to experimental ones for liquid SiO_2.

DOI: 10.1103/PhysRevB.70.134204 PACS number(s): 78.55.Qr, 61.43.Bn

I. INTRODUCTION

Liquid and amorphous Al_2O_3 have been investigated intensively by both experiment and computer simulation. Al_2O_3 is an important ceramic material and amorphous Al_2O_3 is found on the surface of most crystal alumina polymorph as well as on the surface of aluminum exposed to air. Atomic-level information about its structure and physical properties would be an important data to understand of the mechanism of the oxidation and passivation processes. The structure of amorphous Al_2O_3 samples was investigated by x-ray and neutron diffraction in Ref. 1, the partial pair correlation functions were determined from computer simulation of structure using the Reverse Monte-Carlo method with the result that amorphous Al_2O_3 is built up by $(AlO_4)^{5-}$ tetrahedra with corner sharing oxygen atoms.[1] El-Mashri and co-workers studied amorphous alumina films by both extended x-ray absorption fine structure and electron extended energy loss fine structure techniques.[2,3] As shown in Refs. 2 and 3 for the porous film the Al–O bond length is 1.9 Å and most Al atoms are octahedrally coordinated. Some authors in Refs. 4 and 5 studied liquid Al_2O_3 through a specially designed laser-heated aerodynamic levitation furnace to obtain the neutron scattering structure factor $S(Q)$ and they constructed a model of liquid Al_2O_3 using the empirical potential structural refinement method and model's $S(Q)$ that is consistent with that determined by neutron scattering. Authors in Refs. 4 and 5 found few of the atomic configurations of α-Al_2O_3 in liquid Al_2O_3. A model of amorphous Al_2O_3 incorporating structural data[6] has been constructed.[7] The model containing 150 particles in a sphere with a diameter of 150 pm. First, particles were arranged quasi-randomly with a limitation on the minimum interparticle distance, coordination number, azimuthal angles and the type of neighbors. Further relaxation of the model was performed by the reverse Monte-Carlo method. In the structure obtained, the distribution of Al-O-Al angles had maxima at 60°, 80°–100° and 120°–130° and the maxima of distribution of O–Al–O angles were at 80°–100°, 130°–140° and 150°–160°. Later, a simulation (500 particles) of liquid (supercooled) at 2000 K and of amorphous Al_2O_3 at 0 K by MD and SR methods with the Born-Mayer pair potentials was done;[8] structural characteristics of models are in good agreement with experiment. Mean coordination numbers are as follows: $Z_{Al-O}=4.47$ and $Z_{O-Al}=2.98$. Some MD simulations regarding structural properties of liquid alumina also performed in Refs. 9–11. Recently the molecular dynamics study of structural properties of amorphous Al_2O_3 has been presented.[12] Simulations were done in ionic models containing 1800 particles, three systems at densities ranging from 3.0 to 3.3 g/cm^3 were prepared by quenching from the melt. The network topology of systems was analyzed through partial pair correlations, coordination numbers, angle distributions and ring statistics with the result that in the amorphous state there is a short-range order dominated by a slightly distorted $(AlO_4)^{5-}$ tetrahedron.

The micro-void structure of amorphous materials has been discussed for a long time; there are some reasons for studies of pores, besides providing a complementary description of the amorphous structure. Large pores may exchange their positions for neighboring atoms[13–24] and therefore behave like vacancies in the diffusion process. The pore in an amorphous structure may be considered as a sphere, which is located in the amorphous solid and does not overlap with the remaining atomic spheres. Publications concerning the pore problem mainly concentrated on the pores in amorphous metals and alloys. Authors in Ref. 13 investigated different kinds of pores in the amorphous model and concluded that a large pore can exchange its position with an atom if its radius is greater than $0.6R_a$, where R_a is the radius of the "atomic sphere." This means that such large pores can play a role of vacancy in diffusion. Similar results were obtained later by Limoge and Delaye, who studied a Lennard-Jones molecular dynamics model.[14] Previously, Vo Van Hoang *et al.* investigated the effects of B and P concentrations on the pore distribution in amorphous Fe-B and Fe-P alloys[23] or in amorphous Co-B and Co-P alloys.[24] They found that the number of large pores in models of amorphous Fe-P and Co-P alloys monotonically increases with phosphorus content. In contrast, the number of large pores in models of amorphous Fe-B and Co-B alloys is rather constant in a wide range of boron concentration and after that it strongly increases. We also can find some works about the pore problem in amor-

phous oxides. The statistics of the pore distribution and the character of their aggregation into bigger pores in amorphous silica were investigated in a model containing 648 ions.[25,26] Pore radii appeared to be in range of 18–183 pm. A series of overlapping pores was considered to be a "tree." It was demonstrated that the number of "trees" decreases rapidly with an increasing of number of pores (N) in a "tree" ($N=3-200$). Recently, Vo Van Hoang *et al.* presented the pore distribution in amorphous SiO_2 models containing 2592 ions.[27] Calculations showed that the size distribution of pores in amorphous SiO_2 is broad specified by the existence of very large pores and the number of large pores increases with temperature. However, problems of pores, of thermodynamics properties of amorphous and liquid Al_2O_3 have not been investigated yet. Therefore, these problems have been studied in this work. The phase transition temperature and thermal expansion coefficient in the Al_2O_3 system were also obtained and presented.

II. CALCULATION

A. Construction of amorphous Al_2O_3

Results of numerous experimental studies of oxide systems indicate a substantial contribution of the ionic bonding to interatomic interactions. This is caused by the high electronegativity of oxygen atoms. Nevertheless, it is important to take accounts of covalent components in the simulation of the structure and properties of oxides. The covalent interaction is described in terms of three-particle potentials, which significantly increases the computational time. Therefore, the models have to be simplified. The choice of a model based only on the ionic interaction has significant advantages. Any doubts in the applicability of the ionic scheme were eliminated in studies, in which a purely ionic model of numerous noncrystalline oxides was successfully built.[28] Therefore, the purely ionic model was used in this work and amorphous Al_2O_3 model containing 3000 ions in a basic cube with periodic boundary conditions was constructed by the SR method at the real density of 3.095 g cm^{-3} for amorphous Al_2O_3. The Born-Mayer type pair potential used here is of the form

$$u_{ij}(r) = z_i z_j \frac{e^2}{r} + B_{ij} \exp\left(-\frac{r}{R_{ij}}\right), \tag{1}$$

where the terms represent Coulomb and repulsion energies, respectively. Parameter r is a distance between the centers of ith and jth ions; z_i and z_j are the charges of ith and jth ions; B_{ij} and R_{ij} are the parameters accounting the repulsion of the ionic shells. Values $z_1=+3$ and $z_2=-2$ are the charges of Al^{3+} and O^{2-}. The values $B_{11}=0$, $B_{12}=1779.86$ eV, $B_{22}=1500$ eV and $R_{ij}=29$ pm were adopted to receive a good agreement with experiment for the partial radial distribution functions (PRDFs) of models, and these parameters are close to the ones used in Ref. 28. Coulomb interactions were taken into account by the Ewald-Hansen method.[28] The calculation of the Coulomb term of energy and interaction forces is to be done by summing according to Ewald, taking into account all particle pairs in the cube (see Refs. 29–32). The procedure of Ewald summation gives high accuracy, but it is computing time consuming. Thus, some approximations were proposed to describe not only spherically symmetrical terms, but also cubic symmetry corrections. Among them, the Hansen approximation[33] represents the interaction energy in the form of exponential-polynomial series giving an error of about 0.1%. Although the Ewald-Hansen approximation loses accuracy, but it leads to a more rapid calculation. The non-Coulomb contribution to the potential was truncated at distance half the length of a basic cube, which is equal about 16 Å. The equilibrium amorphous model was reached after 6000 SR steps from the random initial configuration of atoms in the basic cube. Further, we have calculated structural characteristics and properties of an obtained model. After that, the model obtained by the SR method at temperature 0 K was "heated up" by the MD method to temperatures in the range from 500 K to 4000 K to study the temperature dependence of structure and thermodynamics properties of liquid and amorphous Al_2O_3. In the liquid state ($T \geqslant 2500$ K), the equilibrium model was reached after 10 000 MD steps.

The static relaxation and molecular dynamics methods involve calculation trajectories of particles under the action of the forces from neighboring particles in the model. In the SR method the system is at zero temperature. The kinetic energy is zero and particles are displaced in the direction in which the resultant force acts. The final SR step was taken about 0.005 Å. For the MD method we used the Verlet algorithm with a time step $\Delta t = 4.0749 \times 10^{-16}$ s.

B. Coordination number distribution

The partial radial distribution functions $g_{ij}(r)$ in a binary system are defined in such a way that, sitting on one atom of species i, the probability of finding one atom of the species j in a spherical shell between r and $r+dr$ is $\rho_j 4\pi r^2 g_{ij}(r)dr$, where $\rho_j = N_j/V$ is the number density of species j, where N_j is the total number of atoms of species j. Useful supplementary information can be obtained by integration around the first peak in the radial distribution functions (RDF), which provides the average coordination number Z_{ij} as given below:

$$Z_{ij}(R) = 4\pi\rho_j \int_0^R g_{ij}(r) r^2 dr, \tag{2}$$

where R is a cutoff radius, usually chosen as the position of the minimum after the first peak in $g_{ij}(r)$. In this work, we choose the same values $R_{Al-Al}=3.70$ Å, $R_{Al-O}=2.2$ Å and $R_{O-O}=3.2$ Å as used in Ref. 12 to calculate coordination number distributions in liquid and amorphous Al_2O_3.

C. Pore distribution

The size distribution of pores surrounding an atom in the model can also be calculated by the method used in Refs. 22–24, 27, and 34 To do this, for the ith atom ($i=1,2,\ldots,N$) we build a three-dimensional cubic lattice with a period of 0.11 Å and a size of 4.9 Å of the ith atom if it is an Al atom, or a lattice with the period of 0.109 Å and a size of 4.7 Å if the ith atom is an oxygen atom.[35] The center of

TABLE I. Structural characteristics of amorphous Al_2O_3. r_{ij}—positions of the first peaks in the partial radial distribution functions (PRDFs) $g_{ij}(r)$; g_{ij}. The heights of the first peaks in PRDFs; Z_{ij}—the average coordination number (1-1 for the Al-Al pair, 1-2 for the Al–O pair, 2-1 for the O-Al pair, 2-2 for the O-O pair).

	r_{ij}(Å)			g_{ij}			Z_{ij}			
	1-1	1-2	2-2	1-1	1-2	2-2	1-1	1-2	2-1	2-2
0 (K)	3.16	1.80	2.77	2.83	9.03	2.60	9.03	4.63	3.09	8.46
500 (K)	3.20	1.79	2.79	3.10	8.32	2.47	8.44	4.47	2.98	8.06
1000 (K)	3.21	1.78	2.79	2.98	7.29	2.45	8.34	4.38	2.93	7.96
1500 (K)	3.20	1.78	2.79	2.99	6.57	2.42	8.34	4.34	2.89	7.84
2000 (K)	3.20	1.77	2.80	2.90	6.06	2.33	8.62	4.23	2.82	7.67
Experimental data (Ref. 1)	3.20	1.80	2.80				6.00	4.10		8.50
Calculation data (Ref. 12)	3.12	1.76	2.75	2.60	8.50	3.50	8.26	4.25		9.47

this lattice is located exactly at the center of the *i*th atom. Then we determine the distance r_{ij} between the *i*th atom and the *j*th node of the lattice and insert a pore sphere with radius $(r_{ij}$-$R_a)$ in the *j*th node, where R_a is the atomic radius of the *i*th atom. Thereby, we have obtained a set of pores with different radii. The next step is to remove the pores, which overlap any atom or have a radius smaller than 0.2 Å because, to our knowledge, such small pores do not play a significant role in structural relaxation. In the case when two pores overlap each other, the smaller one must be removed. This means that an elementary pore is defined as the largest spherical volume that can be inserted into a set of some atoms surrounding the central *i*th atom, touching all of them, such that no other atom lies within the spherical region. The radius of Al atom is taken equal to 125 pm (see in Ref. 36) and of an oxygen atom equal to 73 pm (see in Ref. 37). At the end of calculations, we can obtain an array of pores that do not overlap with each other or any surrounding atoms.

D. Pressure calculation and keeping pressure constant

Pressure in the model, p, is calculated in two terms through Coulomb interaction and short range interaction by equation: $p=p_c+p_s$. As to the Coulomb term, the pressure is calculated using the equation

$$p_c V = \frac{E_{Coulomb}}{3}, \tag{3}$$

where V is the volume of model; $E_{Coulomb}$ is the total Coulomb interaction energy of the model and p_c is the Coulomb term of pressure.

For the short range interaction term, we use the virial formula[38] as given below:

$$p_s V = \frac{\sum_{i,j} r_{ij} \cdot F_{ij}}{3}, \tag{4}$$

where r_{ij} is the distance between the *i*th atom and the *j*th atom; F_{ij} is the short range interaction forces and p_s is the short range interaction term of pressure. The sum is taken over all pairs of atoms.

All calculations in this work were carried out under constant pressure ($p=0$ GPa). Zero pressure is established using the size correction of the basic cube. We may simulate the model at different cube sizes and find the true size by interpolation to the zero pressure. Indeed, the pressure fluctuates in the MD run but we can establish the mean pressure to be almost equal to zero.

III. RESULTS AND DISCUSSION

A. Structural characteristics of amorphous Al_2O_3

Table I and Fig. 1 show structural characteristics of the Al_2O_3 in our simulations and they are very close to the experimental data of Ref. 1 and to the calculated data in Ref. 12. The PRDFs agree well with calculated PRDFs in Ref. 12 in terms of the shape, position and amplitude of the peaks. It is essential to notice that the neutron static structure factor $S_N(q)$ and the x-ray structure factor $S_x(q)$ in Ref. 12 almost completely fit the experimental curves in Ref. 1. We also display the calculated total neutron-weighted pair-distribution function $g_N(r)$ for amorphous Al_2O_3, defined by

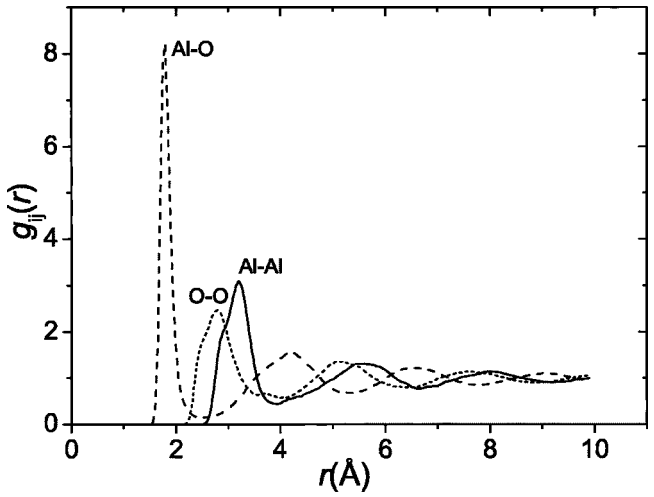

FIG. 1. Partial radial distribution functions of an amorphous Al_2O_3 model at a temperature of 500 K.

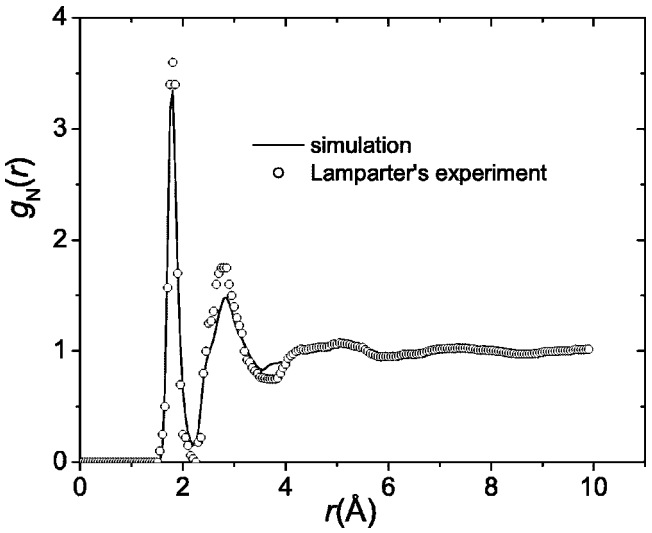

FIG. 2. Total neutron radial distribution function $g_N(r)$ of amorphous Al_2O_3 model at a temperature of 500 K.

$$g_N(r) = \frac{x_1^2 f_1^2 g_{11}(r) + 2x_1 x_2 f_1 f_2 g_{12}(r) + x_2^2 f_2^2 g_{22}(r)}{(x_1 f_1 + x_2 f_2)^2}, \quad (5)$$

where $x_i = N_i/N$ is the concentration of the ith species and f_i is the corresponding coherent neutron scattering length. As described above, number 1 is described for an aluminum atom and number 2 is for an oxygen atom. We take $f_{Al} = 0.3449 \times 10^{-14}$ m and $f_O = 0.5805 \times 10^{-14}$ m as used in Ref. 12. Figure 2 shows that our calculated $g_N(r)$ is close to the experimental one obtained by Lamparter and Kniep[1] and with the calculated data in Ref. 12. Although the calculated $g_N(r)$ does not agree well with the experimental one, especially for the heights of the 1st two peaks, but there is some coincidence in the position of the first two peaks, which are located at 180 pm and 280 pm in the experimental pair distribution function (PDF), and at 180 pm and 282 pm in our computed PDF.

Small decreases in the heights of peaks in the PRDFs, g_{ij}, and of the average coordination number Z_{ij} with increasing temperature had been obtained (see Table I). As presented in Refs. 1 and 12 amorphous Al_2O_3 has the structure of a tetrahedral network with the average coordination number $Z_{Al-O} \approx 4$. The structural element of network is a slightly distorted $(AlO_4)^{5-}$ tetrahedron. The same structure also exists in our models (see Table I).

We can see the tetrahedral network structure of models of amorphous Al_2O_3 through the coordination number distribution of Al^{3+} ions for the pair Al–O at different temperatures (Table II). As shown in Table II, Al atoms are mainly surrounded by four oxygen atoms and the fraction of Al atoms having threefold and fourfold coordinations increases with increasing temperature. In contrast, the number of Al atoms having a coordination number equal to 5 and 6, decreases. At temperatures $T \geqslant 1000$ K we obtained the occurrence of Al atoms having only twofold coordination, although their number increases with increasing temperature, their fraction is very small.

TABLE II. Coordination number distribution for the pair Z_{Al-O} in an amorphous state.

Z_{Al-O}	2	3	4	5	6
Number of Al^{3+} ions (at $T=0$ K)	0	2	496	643	59
Number of Al^{3+} ions (at $T=500$ K)	0	11	643	516	30
Number of Al^{3+} ions (at $T=1000$ K)	1	15	711	450	23
Number of Al^{3+} ions (at $T=1500$ K)	0	34	734	408	16
Number of Al^{3+} ions (at $T=2000$ K)	2	89	750	347	12

Figure 3 presented coordination number distributions in an amorphous Al_2O_3 model at the temperature of $T=500$ K; these distributions are broad and close to the same distributions obtained in Ref. 12. Important information about the local structural units is provided by the angle distribution. As displayed in Ref. 12, the O–Al–O bond angle distribution has a peak at 104°, O-O-O has a main peak at 60°, Al-O -O presents a main peak at 39° and Al-O-Al distribution has a peak at 120°. These calculated angle distributions are very close to the calculated data in Ref. 6. In this work, we do not calculate angle distributions again, but from the average interatomic distances r_{Al-O} and r_{Al-Al} the average Al-O-Al bond angle between two corner sharing tetrahedra results is about 126.70° and close to the value of the angle obtained in Ref. 1. Also, from the r_{Al-O} and r_{O-O}, the calculated average O-Al-O and Al-O-O bond angles are about 102.40° and 38.8°, respectively. It is essential to notice that Lamparter and Kniep also calculated the average bond-angles through average interatomic distances as it was done here (see Ref. 1). It is well known that for an ideal tetrahedron, the O-Al -O bond angle is equal to 109.47°. Our results have a small deviation from this value, but they are very close to the same angles in Ref. 12 (see above). Combining this information with the interatomic distances and coordination numbers, we confirm that the elementary unit of the Al_2O_3 system consists of a distorted $(AlO_4)^{5-}$ tetrahedron. The other basic units are fivefold or sixfold coordinated polyhedra AlO_5 and AlO_6, but the fraction of AlO_6 is small and decreases with increasing

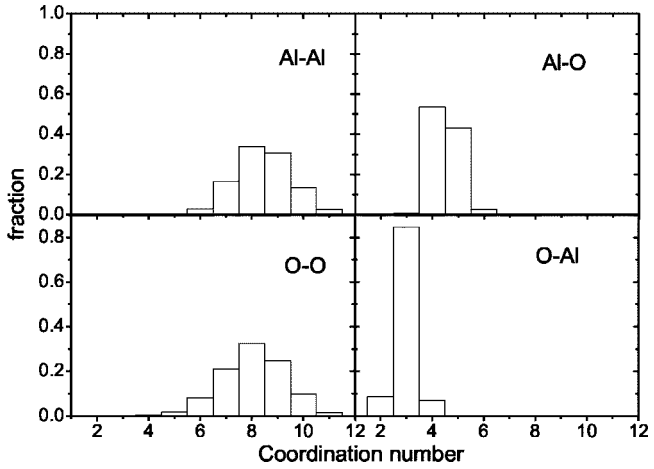

FIG. 3. Coordination number distribution in the amorphous Al_2O_3 model at $T=500$ K.

TABLE III. Size distribution of pores in amorphous Al_2O_3 models. R is the radius of pores; numbers in the next columns show the average number of pores surrounding each atom (Al or O) in models at different temperatures. For example, at temperature 0 K there are 6.3017 pores or 1.6522 pores surrounding each Al or O atom, respectively, with the radius in the range of 0.2–0.3 Å.

	$T=0$ K		$T=500$ K		$T=1000$ K		$T=1500$ K		$T=2000$ K	
R (Å)	Al	O	Al	O	Al	O	Al	O	Al	O
0.2–0.3	6.3017	1.6522	6.0350	1.5783	6.0717	1.5711	5.9691	1.5972	5.8400	1.5678
0.3–0.4	2.4992	0.7955	2.4842	0.7633	2.6342	0.7705	2.5492	0.7900	2.5383	0.8183
0.4–0.5	1.1492	0.6500	1.1950	0.6339	1.108	0.6011	1.2200	0.5800	1.1925	0.5678
0.5–0.6	0.9917	0.6317	0.8808	0.5539	0.8642	0.5650	0.8800	0.5139	0.8942	0.5033
0.6–0.7	1.0333	0.5422	0.8175	0.4461	0.8267	0.4067	0.8158	0.4694	0.8208	0.4494
0.7–0.8	0.9992	0.4561	0.7825	0.3394	0.8017	0.3800	0.7817	0.3800	0.7992	0.3905
0.8–0.9	0.9442	0.4350	0.7767	0.3739	0.7392	0.3594	0.7408	0.3544	0.8017	0.3555
0.9–1.0	0.8317	0.4033	0.6892	0.3405	0.6908	0.3728	0.7142	0.3539	0.6517	0.3628
1.0–1.1	**0.6708**	**0.2650**	**0.6275**	**0.2994**	**0.6542**	**0.3011**	**0.6408**	**0.3244**	**0.6442**	**0.3155**
1.1–1.2	**0.5375**	**0.2172**	**0.5583**	**0.2722**	**0.5958**	**0.2772**	**0.5533**	**0.2733**	**0.5992**	**0.2667**
1.2–1.3	**0.3383**	**0.1450**	**0.4875**	**0.2155**	**0.4817**	**0.2233**	**0.4767**	**0.1872**	**0.4283**	**0.2139**
1.3–1.4	**0.2692**	**0.0705**	**0.4483**	**0.1261**	**0.4825**	**0.1267**	**0.5042**	**0.1505**	**0.5433**	**0.1472**
1.4–1.5	**0.1967**	**0.0417**	**0.4558**	**0.0867**	**0.4250**	**0.0844**	**0.4458**	**0.0878**	**0.4592**	**0.0878**
1.5–1.6	**0**	**0.0300**	**0**	**0.0600**	**0**	**0.0667**	**0**	**0.0517**	**0**	**0.0600**
1.6–1.7	**0**	**0.0367**	**0**	**0.0678**	**0**	**0.0633**	**0**	**0.0767**	**0**	**0.0800**
1.7–1.8	**0**	**0**	**0**	**0**	**0**	**0**	**0**	**0**	**0**	**0**
1.8–1.9	**0**	**0**	**0**	**0**	**0**	**0**	**0**	**0**	**0**	**0**
1.9–2.0	**0**	**0**	**0**	**0**	**0**	**0**	**0**	**0**	**0**	**0**

temperature. The threefold coordinated polyhedra also exist, but their fraction is small and increases with temperature.

B. Pore distribution in amorphous Al_2O_3 models

The distribution of pores surrounding an atom in amorphous Al_2O_3 models at different temperatures was presented in Table III. We can see that the distributions are broad and pore radii appeared to be in the range of 20–170 pm. The average number of large pores in models (with the radii $R \geqslant 100$ pm) increases with temperature like that one in amorphous SiO_2 models (see Ref. 27 and Fig. 4). The existence of large pores with radius $R \geqslant R_a$ (R_a–the atomic radius) in models was obtained. These pores can freely receive neighbor atoms and participate in the diffusion process and they can play a role of vacancies like that in crystalline materials. In amorphous metals and alloys, pores with radius $R \geqslant 0.6R_a$ can play the role of vacancies.[20–24] The size distribution of pores in amorphous Al_2O_3 models differs from the one in amorphous models of metallic alloys[20–24] by the larger width of distribution and by the existence of very large pores (with the radius larger than the atomic radius). The existence of large pores in amorphous Al_2O_3 models indicates the loose structure of material.

As seen in Table III, the total weight of such large pores surrounding each Al atom with radius $R \geqslant 1.0$ Å is equal to 2.012, 2.577, 2.639, 2.621 and 2.674 at temperatures of 0 K, 500 K, 1000 K, 1500 K and 2000 K, respectively (the total amount of the bold numbers in each column in Table III). Meanwhile, those numbers for each oxygen atom are equal about 0.806, 1.128, 1.143, 1.152 and 1.171 (e.g., 806, 1128, 1143, 1152 and 1171 large pores in the model containing 1000 oxygen atoms on average). This means that the number of large vacancy-like pores increases with temperature [see Fig. 4(a)]. In contrast, it seems that the number of small pores (with the radius $R \leqslant 0.5$ Å) decreases with temperature [see Fig. 4(b)]. Because the statistical error is very small (less than 10^{-4}) the error bar is not added to the data in Table IV and Fig. 4.

The SR amorphous model corresponds to an amorphous system at the temperature 0 K, so that we may regard the large pores in the model of Al_2O_3 at 0 K as "native" vacancies related to the disorder degree of an amorphous state. When the temperature increases, thermally activated vacancies may occur, the number of which must depend on temperature and on the distribution of formation energy. The existence of large pores ensures the possibility of a vacancy diffusion mechanism in amorphous Al_2O_3. Hence, the self-diffusion of Al, O atoms via a vacancy diffusion mechanism in amorphous Al_2O_3 may take place via both processes.

C. Thermodynamics properties of amorphous Al_2O_3

Table IV presents thermal characteristics of amorphous Al_2O_3 models at different temperatures and at constant pressure ($P \approx 0$ GPa). We can see that the length of the basic cube, L, increases linearly with temperature according to the equation below:

$$L = L_0(1 + \alpha T). \tag{6}$$

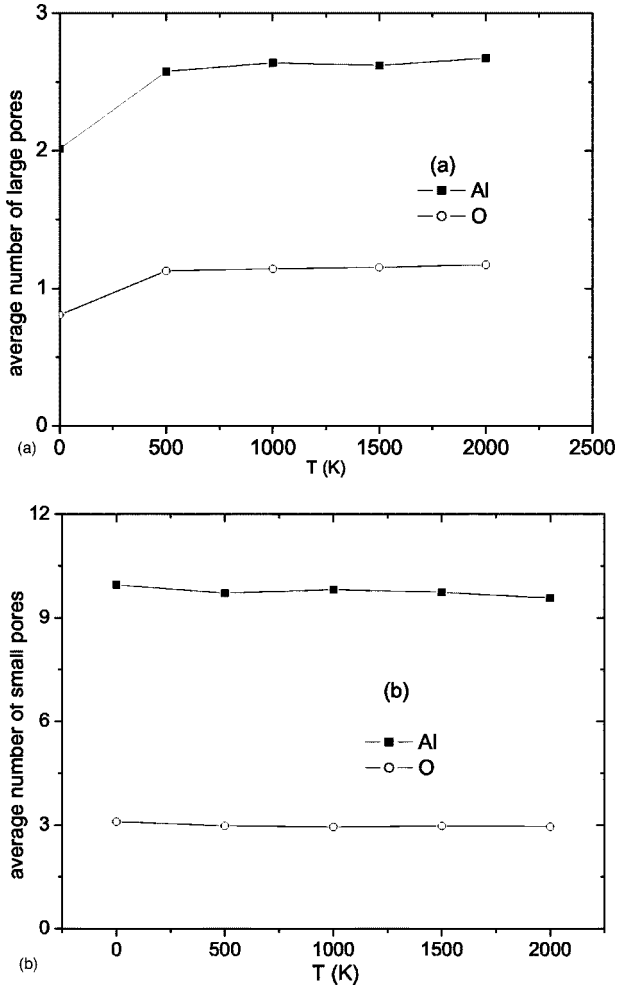

FIG. 4. (a) Temperature dependence of the average number of large pores (with radius $R \geqslant 1.0$ Å) surrounding an atom (Al or O) in amorphous Al_2O_3 models. (b) Temperature dependence of the average number of small pores (with radius $R \leqslant 0.5$ Å) surrounding an atom (Al or O) in amorphous Al_2O_3 models.

The calculated coefficient of thermal expansion $\alpha \approx 4.65 \times 10^{-6}$ K^{-1} and it is very close to the experimental value of crystalline Al_2O_3 $\alpha \approx 5.4 \times 10^{-6}$ K^{-1} (see Ref. 39). Table IV also shows the temperature dependence of the length of basic cube of our model and values predicted by Eq. (6). We can see that the values predicted by Eq. (6) agree well with simulation. There is small deviation at the temperature of 0 K, possibly, related to the less stable state of an amorphous model obtained by the SR method. The energy of the model at the temperature of 0 K is about −14 997 kJ mol^{-1} and is close to the atomization energy of real crystal Al_2O_3, which is equal to −15300 kJ mol^{-1} (see Ref. 28). This means that such Born-Mayer potential exhibits the atomization energy of a system well. Values of the different contributions to the cohesive energy of a system at different temperatures are also presented in Table IV. We can see that the Coulomb interaction has the largest contribution to the cohesive energy of system. And the attractive interaction between Al^{3+} and O^{2-} ions is stronger than either the Al-Al or O-O interactions (see $E_{pair\ Coulomb\ energy}$ in Table IV). It is essential to notice that the total repulsive energy for the pair Al-Al is equal to zero and it has not been presented in Table IV.

The average heat capacity for this temperature region has a reasonable value $C_p = 110$ JK^{-1} mol^{-1} (which is obtained by making use of $C_p = \Delta E_{total}/\Delta T$). The order of the phase transformation from liquid to amorphous states was the subject of numerous studies. The order of the phase transformation can be defined from a thermodynamic standpoint by a number of changes in material properties at the transition temperature T_g (e.g., the changes in enthalpy, in heat capacity, in specific volume, …). The most popular point of view is that the liquid-amorphous transition is not a true second order transition but only a "pseudo" second order phase transition. For the simulated ionic system KCl,[40] the sudden changes in the derivative of the volume-temperature isobaric plot and the enthalpy-temperature isobaric plot in the region of $0.3T_m$ are characteristics of an experimental glass transition, where T_m is the melting point. Even for small size systems, it takes a long million MD run to obtain the order of the phase transition from the liquid to amorphous Al_2O_3. Therefore, in this work, the order phase transition could not be studied and it will be the object of future studies. On the other hand, the transition temperature T_g may also be determined by the extrapolation of the temperature dependence of a self-diffusion constant of Al and O atoms in the liquid Al_2O_3 models (see below).

D. Structure and static properties of liquid Al_2O_3

Alumina melts at a temperature of (2326±8)K (see Ref. 4) and liquid alumina has attracted attention from both ex-

TABLE IV. Thermal characteristics of models of amorphous Al_2O_3. L—the length of basic cube; $E_{pair\ repulsive}$—the total repulsive energy of different pairs of ions in the model; $E_{pair\ Coulomb}$—the total Coulomb energy of different pairs of ions in the model; $E_{Coulomb}$—the total Coulomb energy of the model; E_{short}—the total energy of the short range interaction of the model; E_{total}—the total energy of the model. (1-1 for the Al-Al pair, 1-2 for the Al–O pair, 2-2 for the O-O pair).

	L(pm)		$E_{pair\ repulsive}$ (in 10^4 eV)		$E_{pair\ Coulomb}$ (in 10^7 eV)			Total energy of model (in 10^5 eV)		
T(K)	Present work	Calculated by Eq. (6)	1-2	2-2	1-1	1-2	2-2	$E_{Coulomb}$	E_{short}	E_{total}
0[a]	3214.20	3270.00	1.549	0.096	0.817	−1.647	0.818	−1.0983	0.1646	−0.9337
500	3278.11	3277.60	1.576	0.087	0.801	−1.614	0.802	−1.0995	0.1663	−0.9312
1000	3284.30	3285.20	1.573	0.086	0.799	−1.611	0.801	−1.0974	0.1658	−0.9277
1500	3291.90	3292.81	1.566	0.085	0.798	−1.608	0.799	−1.0948	0.1651	−0.9238
2000	3301.51	3300.41	1.565	0.084	0.795	−1.603	0.797	−1.0927	0.1649	−0.9200

[a]The model at the temperature of 0 K has been obtained by the SR method.

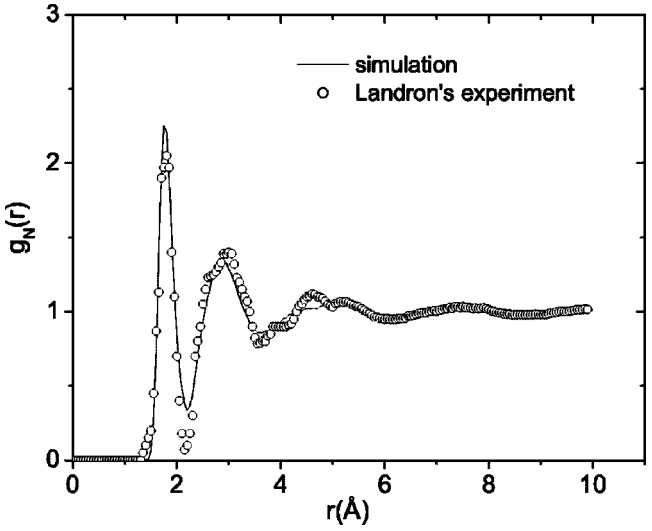

FIG. 5. Total neutron radial distribution function of a liquid Al_2O_3 model at a temperature of 2500 K.

periment and theory. Liquid alumina is a standard reference material in high temperature applications and an understanding of its properties is essential for materials processing.[41] However, the structure and properties of liquid Al_2O_3 have been less studied because it is very difficult to carry out experiments at very high temperatures. Some structural characteristics of liquid Al_2O_3 have been obtained by Landron's group and Gutierrez.[4,5,11] In this work, the static and dynamic properties of liquid Al_2O_3 were studied for a wide range of temperatures from 2500 K to 4000 K by the MD method. At temperature 2500 K, the calculated total neutron distribution function $g_N(r)$ agrees well with the experimental one (see Fig. 5).

Table V shows that calculated partial radial distribution functions $g_{ij}(r)$ of the model at a temperature of 2500 K agree well with experimental ones for the positions of first peaks. Calculated average coordination number Z_{12} is equal to 4.16 and close to experimental data in Ref. 4 which is equal to 4.2 ± 0.3. At an almost high temperature of 4000 K, the coordination number $Z_{12}\approx4$. This means that the structure of liquid alumina is tetrahedral-like silica. The length of a basic cube of the model at a temperature of 2500 K is equal to 33.096 Å, the corresponding density is 2.80 g cm^{-3}, which is close to the value of 2.81 g cm^{-3} measured directly

TABLE VI. Coordination number distribution for the pair Z_{Al-O} in a liquid state.

Z_{Al-O}	2	3	4	5	6
Number of Al^{3+} ions (at $T=2500$ K)	3	124	754	310	9
Number of Al^{3+} ions (at $T=3000$ K)	5	169	794	227	5
Number of Al^{3+} ions (at $T=3500$ K)	15	242	770	168	5
Number of Al^{3+} ions (at $T=4000$ K)	22	315	726	133	4

in Ref. 5. A number of molecular dynamics studies of liquid alumina have been made[9–11] including a simulation of the γ-Al_2O_3 radial distribution function, which bears some similarity with the supercooled state.[42] In all cases, the densities employed were higher than the density used in this work and in Refs. 4 and 5. Thus, while there are broad similarities between PRDFs of these simulations there are also significant differences.[43] The calculated coordination number $Z_{12}=4.16$ at the temperature of 2500 K compares well with a value of 4.4 ± 1.0 atoms reported by Ansell *et al.* (see Ref. 44). Ansell *et al.* interpreted their data in terms of a transition from octahedron coordination in the solid to tetrahedral coordination of Al atoms in liquid alumina, whereas Waseda *et al.*[45] concluded that the octahedral coordinated aluminum in corundum is retained in the liquid. The NMR data[46] indicated that liquid alumina consisted of a mixture of 4-fold and 6-fold coordinated Al sites undergoing rapid exchange, resulting in the average coordination number 4.5. Poe *et al.*[9] suggested the presence of 5-fold coordinated Al in liquid alumina and the mean coordination number being the average of 4-, 5- and 6-fold sites.[46] As shown in Table VI, there is a distribution of coordination numbers between 2 and 6 oxygen atoms about aluminum for all ranges of temperatures from 2500 K to 4000 K, but the fractions of 2-fold and 6-fold coordinations are small. The number of AlO_4 tetrahedral coordination units increases and then decreases slightly with increasing temperature, we can consider that AlO_3 and AlO_5 units are being the defects in liquid alumina. The number of AlO_3 units increases with temperature and at low temperatures ($T\leqslant3250$ K) it shows an Arrhenius law $P_{ij}=A_{ij}\exp(-E_{ij}/T)$, where P_{ij} is the probability for the occurrence of such defects[47] (see Fig. 6). For the case of $Z_{12}=3$ we find that pre-factor $A_{12}=0.9423$ and activation energy $E_{12}=5654$ K. In the liquid SiO_2 (see Ref. 47) for the same $Z_{12}=3$ they found that $A_{12}=58.6$ and $E_{12}=31100$ K. In contrast,

TABLE V. Structural characteristics of liquid Al_2O_3. r_{ij}—positions of the first peaks in the partial radial distribution functions (PRDFs) $g_{ij}(r)$; g_{ij}—the heights of the first peaks in PRDFs; Z_{ij}—the average coordination number (1-1 for the Al-Al pair, 1-2 for the Al−O pair, 2-1 for the O-Al pair, 2-2 for the O-O pair).

	r_{ij} (Å)			g_{ij}			Z_{ij}			
	1-1	1-2	2-2	1-1	1-2	2-2	1-1	1-2	2-1	2-2
2500 (K)	3.20	1.77	2.80	2.73	5.60	2.23	8.07	4.16	2.78	7.48
3000 (K)	3.22	1.75	2.81	2.66	5.33	2.13	7.70	4.05	2.70	7.12
3500 (K)	3.23	1.75	2.79	2.49	5.09	2.09	7.47	3.92	2.61	6.85
4000 (K)	3.21	1.74	2.77	2.43	4.92	2.00	7.06	3.82	2.54	6.55
Experimental data (Refs. 4 and 5) at 2473 (K)	3.25	1.78	2.84	1.70	5.60	2.40		4.20		

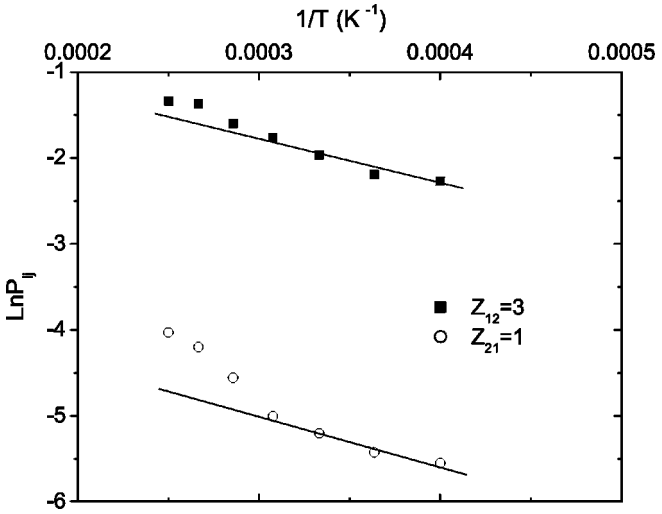

FIG. 6. Temperature dependence of the probability for the occurrence of defects, P_{ij}, for the cases of partial coordination numbers $Z_{12}=3$ and $Z_{21}=1$.

the number of AlO_5 units decreases. Analogously, for the coordination pair O-Al, the number of defects $Z_{21}=1$ also increases with temperature and shows an Arrhenius law (see Fig. 6) with $A_{21}=0.041$ and $E_{21}=5955$ K.

E. Self-diffusion in liquid Al_2O_3 models

If the interparticle potential is known, it is easy to calculate self-diffusion constants of a liquid by the molecular dynamics method. In the process of the molecular dynamics relaxation of the liquid phase, the particles of the model at each temporal step perform small displacements correlated with displacements of neighboring particles. Hence, the cooperative diffusion mechanism is realized. The self-diffusion constants of ions in the liquid Al_2O_3 model can be determined through the mean squared particle displacement $\langle r^2 \rangle$ via the Einstein relation:

$$D = \lim_{t \to \infty} \frac{\langle r^2(t) \rangle}{6t}. \tag{7}$$

Liquid Al_2O_3 model at $T \geqslant 2500$ K can be obtained by "heating up" the 2000 K amorphous Al_2O_3 model through a long MD relaxation (after 10 000 MD time steps) to reach a good equilibrium liquid state. Then at each temperature we can determine diffusion constants D after another 10000 MD time steps. The time dependence of $\langle r^2 \rangle$ was presented in Fig. 7.

The obtained diffusion constant D for Al^{3+} ions ranged from $(0.36 \pm 0.01) \times 10^{-5}$ cm^2 s^{-1} to $(4.12 \pm 0.07) \times 10^{-5}$ cm^2 s^{-1} at the temperatures from 2500 K to 4000 K, respectively. Meanwhile, those numbers for the O^{2-} ions ranged from $(0.53 \pm 0.02) \times 10^{-5}$ cm^2 s^{-1} to $(5.28 \pm 0.08) \times 10^{-5}$ cm^2 s^{-1} for the same temperature range (see Fig. 8). This means they have reasonable values and close to the calculated values D for ions Si^{4+} and O^{2-} in liquid SiO_2 models.[40,47] The temperature dependence of self-diffusion constants D in liquid Al_2O_3 models shows an Arrhenius law (see Fig. 9) as given below:

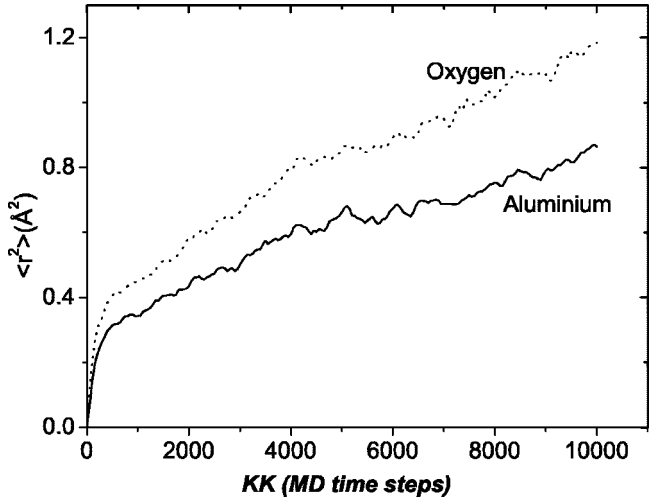

FIG. 7. Time dependence of the mean squared displacement of a particle at $T=2500$ K.

$$D = D_0 \exp\left(-\frac{E}{k_B T}\right). \tag{8}$$

For Al^{3+} ions, the pre-exponential constant $D_0 \approx 2.478 \times 10^{-5}$ cm^2 s^{-1} and activation energy at constant pressure $E \approx 1.40$ eV. For O^{2-} ions, the pre-exponential constant $D_0 \approx 2.739 \times 10^{-5}$ cm^2 s^{-1} and the corresponding activation energy at constant pressure $E \approx 1.32$ eV. For liquid SiO_2 (see Ref. 47), they found that the activation energies are 4.66 eV and 5.18 eV for oxygen and silicon, respectively. These numbers compare well with the ones determined in experiments at significantly lower temperatures, namely, 4.7 eV for oxygen[48] and 6 eV for silicon.[49] For liquid alumina the experimental data was not found, but we can see that the calculated data have reasonable values. Such an excellent agreement between the theoretical and experimental activation energies for liquid SiO_2 is not trivial as it has recently been demonstrated by Hemmati and Angell,[50] who showed that various models for silica can give rise to quite different activation energies. These authors showed that different models

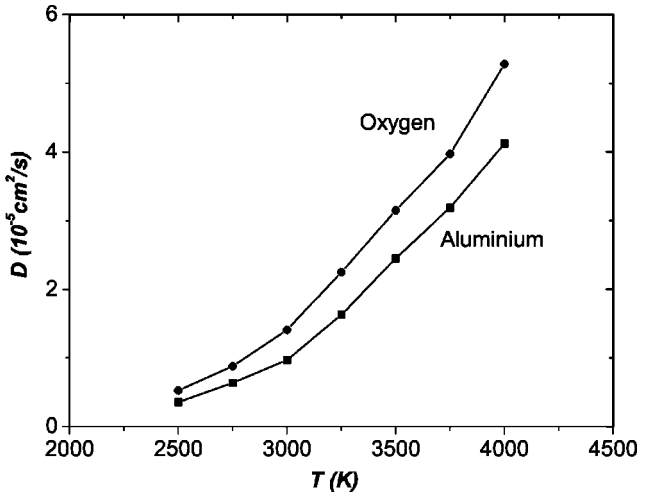

FIG. 8. Temperature dependence of self-diffusion coefficients.

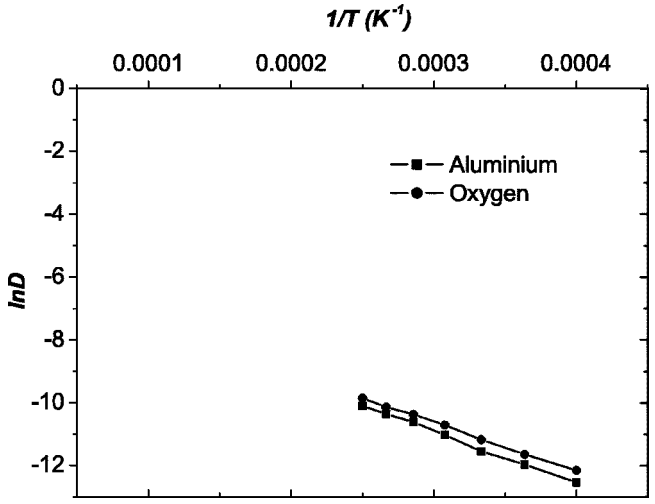

FIG. 9. The $1/T$ dependence of ln D.

predict diffusion constants which differ by up to two decades at temperatures as high as 3000 K, which show that dynamical quantities such as D depend much more sensitively on the potential than structural quantities. For higher temperatures, significant deviations from the Arrhenius law were obtained for liquid SiO_2 (see Ref. 47) that the diffusion constants increase more slowly with increasing temperature than expected from an activated process. Recently, Hess *et al.* have reported the analysis of experimental viscosity data of SiO_2 at high temperatures and find that deviations from a pure Arrhenius law are present.[51] Such a problem will be investigated in more detail for the liquid alumina in future studies.

In order to quantify the difference in the temperature dependence of different diffusion constants, we can find that the ratio D_{Al}/D_O for liquid alumina varies only from 0.68 to 0.78 in the temperature range of 2500 K$\leqslant T\leqslant$4000 K and it is very similar to that ones in liquid SiO_2, where the ratio D_{Si}/D_O varies from 0.65 to 0.80 in the temperature range of 3400 K$\leqslant T\leqslant$6100 K (see Ref. 52). This means that in liquid SiO_2 and Al_2O_3, ions O^{2-} diffuse faster than ions Si^{4+} or Al^{3+} but the difference is small and is contrary to the results obtained in Ref. 52. They found that in liquid $(Al_2O_3)2(SiO_2)$ at $T=6100$ K the temperature dependences of diffusion constants $D(T)$ are very similar to those in SiO_2 (e.g., to those in our Al_2O_3). However, upon decreasing the temperature, the dynamics in $(Al_2O_3)2(SiO_2)$ does not slow down as rapidly as the one of SiO_2. At $T=2750$ K the diffusion of all components in $(Al_2O_3)2(SiO_2)$ is about two orders of magnitude faster than in SiO_2. They explained that the self-diffusion constants in SiO_2 show a crossover from a power law behavior as predicted by the mode-coupling theory of the glass transition[53] at high temperatures to an Arrhenius behavior at low temperatures whereby they found the critical mode-coupling temperature at 3330 K (see Refs. 47 and 54). The so-called mode-coupling theory[55] related the slowing down of the dynamics upon cooling to nonlinear feedback effects, is able to give a qualitative and quantitative correct descriptions of glass formers in which the interaction between particles is not too different from the one of a hard-sphere system, such as a colloidal system,[56] the molecular glass-former orthoterphenyl,[57] and even systems in which some hydrogen bonding is present, such as glycerol.[58] The main prediction of the theory is that there exists a critical temperature T_c at which the relaxation dynamics of the system changes qualitatively in that an unexpectedly fast increase of the local activation energy of the transport coefficients, such as the viscosity or the inverse of the diffusion constant, is observed.

Results of self-diffusion study in $(Al_2O_3)2(SiO_2)$ also provide the very interesting case of a tetrahedral network where the dynamics of one of the cations, aluminum, is slightly faster than that of oxygen whereas the diffusion of the other cation, silicon, is a factor of 2 or 3 slower than that of oxygen. We investigated the self-diffusion in liquid Al_2O_3 in temperature range from 2500 K to 4000 K (e.g., at the low temperature region for the liquid Al_2O_3) and it may be below the critical mode-coupling temperature for Al_2O_3 system. Therefore, the diffusion of all components in $(Al_2O_3)2(SiO_2)$ is possibly faster than in our Al_2O_3 system like those for liquid SiO_2. This fact exhibits the physical phenomena that one encounters in multicomponents melts. Furthermore, our calculated oxygen diffusion constant D_O is greater than the aluminum diffusion constant D_{Al} and is contrary to the results in Ref. 52, possibly, relates to the different potentials used in our work and in Ref. 52 because dynamical quantities such as D are much more sensitively on the potential than structural quantities.[50] This problem may be checked in future studies.

As noticed above the phase transition temperature T_g for the Al_2O_3 system also can be found by the extrapolation from the temperature dependence of diffusion constants D (Fig. 9) and this is equal to about 2000 K.

IV. CONCLUSIONS

Structures of the liquid and amorphous Al_2O_3 models constructed by the *SR* and *MD* methods using an ionic model with Born-Mayer type pair potentials are in good agreement with experimental data. Calculations showed that in the liquid and amorphous states there is a short-range order dominated by a slightly distorted $(AlO_4)^{5-}$ tetrahedron. The pore distributions in amorphous Al_2O_3 models are broad. The number of large pores increases with increasing temperature, whereas the number of small pores decreases. The phase transition temperature from liquid to amorphous states for an Al_2O_3 system has been determined at anywhere around 2000 K. The calculated thermal expansion coefficient of an amorphous Al_2O_3 model is close to that of crystalline Al_2O_3. Calculated self-diffusion constants for Al^{3+} and O^{2-} in liquid Al_2O_3 have reasonable values which are close to the data for the SiO_2 system. At temperatures $T\leqslant$4000 K the temperature dependence of the diffusion constants shows an Arrhenius law with activation energies which have reasonable values.

ACKNOWLEDGMENTS

I thank Professors D. K. Belashchenko and Suhk Kun Oh for helpful comments to the manuscript.

*Electronic address: vvhoang@phys.hcmuns.edu.vn

[1] P. Lamparter and R. Kniep, Physica B **234**, 405 (1997).
[2] S. M. El-Mashri, R. G. Jones, and A. J. Forty, Philos. Mag. A **48**, 665 (1983).
[3] A. J. Bourdillon, S. M. El-Mashri, and A. J. Forty, Philos. Mag. A **49**, 341 (1984).
[4] C. Landron, A. K. Soper, T. E. Jenkins, G. N. Greaves, L. Hennet, and J. P. Coutures, J. Non-Cryst. Solids **293–295**, 453 (2001).
[5] C. Landron, L. Hennet, T. E. Jenkins, G. N. Greaves, J. P. Coutures, and A. K. Soper, Phys. Rev. Lett. **86**, 4839 (2001).
[6] I. A. Popova, Neorg. Mater. **14**, 1934 (1978).
[7] V. M. Kozlov, I. A. Popova, and T. A. Shabalina, Izv. Akad. Nauk. Latv. SSR, Ser. Fiz. Tech. Nauk. **3**, 73 (1982).
[8] D. K. Belashchenko, Neorg. Mater. **27**, 2127 (1991).
[9] B. T. Poe, P. F. McMillan, B. Cote, D. Massiot, and J. P. Coutures, J. Phys. Chem. **96**, 8220 (1992).
[10] M. A. SanMiguel, J. F. Sanz, L. J. Alvarez, and J. A. Odriozola, Phys. Rev. B **58**, 2369 (1998).
[11] G. Gutiérrez, A. B. Belonoshko, R. Ahuja, and B. Johansson, Phys. Rev. E **61**, 2723 (2000).
[12] G. Gutiérrez and B. Johansson, Phys. Rev. B **65**, 104202 (2002).
[13] P. K. Hung and D. K. Belashchenko, Izv. Vusov-Chior. Metall. **1**, 91 (1987).
[14] J. M. Delaye and Y. Limoge, J. Phys. I **3**, 2079 (1993).
[15] D. K. Belashchenko and P. K. Hung, Izv. Vusov-Chior. Metall. **9**, 81 (1986).
[16] P. K. Hung, P. N. Nguyen, and T. B. Van, in Proceedings of the International Workshop for Materials Science, Hanoi, Vietnam, 1995, p. 456.
[17] P. K. Hung, D. K. Belashchenko, and P. N. Nguyen, Russ. Metall. **4**, 155 (1996).
[18] C. N. Bennet, P. Chaudhani, V. Moruzzi, and P. Steinhardt, Philos. Mag. A **40**, 485 (1979).
[19] T. Egami, K. Maeda, and V. Vitek, Philos. Mag. A **41**, 883 (1980).
[20] Vo Van Hoang, Ph.D thesis, Moscow Steel and Alloys Institute, 1991.
[21] Vo Van Hoang, T. B. Van, and P. K. Hung, J. Metastable Nanocryst. Mater. **2–6**, 551 (1999).
[22] Vo Van Hoang and T. B. Van, J. Metastable Nanocryst. Mater. **9**, 5 (2001).
[23] Vo Van Hoang, J. Phys. B **348**, 347 (2004).
[24] Vo Van Hoang, N. H. Hung, and N. H. Tuan Anh, J. Metastable Nanocryst. Mater. **18**, 43 (2003).
[25] S. L. Chan and S. R. Elliott, Phys. Rev. B **43**, 4423 (1991).
[26] S. N. Taraskin, S. R. Elliott, and M. I. Klinger, J. Non-Cryst. Solids **263**, 192 (1995).
[27] Vo Van Hoang, D. K. Belashchenko, and V. T. Mai Thuan, J. Phys. B **348**, 249 (2004).
[28] D. K. Belashchenko, Russ. Chem. Rev. **66**, 733 (1997).
[29] D. J. Adams and I. R. McDonald, J. Phys. C **7**, 2761 (1974).
[30] F. Lantelme, P. Turq, B. Quentrec, and J. W. Lewis, Int. J. Mod. Phys. A **28**, 1537 (1974).
[31] J. Kieffer and C. A. Angell, J. Chem. Phys. **90**, 4982 (1989).
[32] M. P. Allen and D. J. Tildesley, *Computer Simulation of Liquids* (Oxford University Press, New York, 1990).
[33] J. P. Hansen, Phys. Rev. A **8**, 3096 (1973).
[34] D. K. Belashchenko, V. V. Hoang, and P. K. Hung, J. Non-Cryst. Solids **276**, 169 (2000).
[35] After extensive testing and comparative studies between different amorphous models of metals or oxides, we have found that if the length of a cubic lattice is about twice the diameter of the central atom one can get good statistical results of pore distribution surrounding an atom. Therefore, the length of 4.90 Å is also good for calculating pores surrounding Co, Fe or Al atoms because of their similar atomic radii, and analogously the length of 4.70 Å is appropriate for B, P or O atoms.
[36] Available at http://www.webelements.com/webelements/elements/text/Al/radii.html
[37] Available at http://www.webelements.com/webelements/elements/text/O/radii.html
[38] V. V. Wood, *Physics of Simple Liquids*, edited by H. N. V. Temperly, J. S. Rowlinson, and G. S. Rushbrooke (North-Holland, Amsterdam, 1968), Part 2.
[39] Available at http://www.superconductivecomp.com/Al2O3subtrates.html
[40] L. V. Woodcock, C. A. Angell, and P. Cheeseman, J. Chem. Phys. **65**, 1565 (1976)
[41] IUPAC Report of Task Force on Secondary Temperature Standards, Rev. Inst. Hautesn Temp. Refact. 1970, Vol. 7, p. 5.
[42] L. J. Alvarez, L. E. Leon, J. F. Sanz, M. J. Capitan, and J. A. Odriozola, J. Phys. Chem. **99**, 17872 (1995).
[43] S. Krishnan and D. L. Price, J. Phys.: Condens. Matter **12**, R145 (2000).
[44] S. Ansell, S. Krishnan, J. K. Richard Weber, J. J. Felten, P. C. Nordine, M. A. Beno, D. L. Price, and M. L. Saboungi, Phys. Rev. Lett. **78**, 464 (1997).
[45] Y. Waseda, K. Sugiyama, and J. M. Toguri, Z. Naturforsch. A **50**, 770 (1995).
[46] P. Florian, D. Massiot, B. Poe, I. Farman, and J. P. Coutures, Solid State Nucl. Magn. Reson. **5**, 233 (1995).
[47] J. Horbach and W. Kob, Phys. Rev. B **60**, 3169 (1999).
[48] J. C. Mikkelsen, J. Appl. Phys. **45**, 1187 (1984).
[49] G. Brebec, R. Seguin, C. Sella, J. Bevenot, and J. C. Martin, Acta Metall. **28**, 327 (1980).
[50] M. Hemmati and C. A. Angell, in *Physics Meets Geology*, edited by H. Aoki and R. Hemley (Cambrige University Press, Cambrige, England, 1998).
[51] K. U. Hess, D. B. Dingwell, and E. Rossler, Chem. Geol. **128**, 155 (1996);E. Rossler, K. U. Hess, and V. N. Novikov, J. Non-Cryst. Solids **223**, 207 (1998).
[52] A. Winkler, J. Horbach, W. Kob, and K. Binder, J. Chem. Phys. **120**, 384 (2004).
[53] W. Gotze and L. Sjogren, Rep. Prog. Phys. **55**, 241 (1992);W. Gotze, J. Phys.: Condens. Matter **10**, A1 (1999).
[54] J. Horbach and W. Kob, Phys. Rev. E **64**, 041503 (2001).
[55] W. Gotze, in *Liquids, Freezing and the Glass Transition*. Proceedings of the Les Houches Summer School of Theoretical Physics, Session LI, 1989, edited by J. P. Hansen, D. Levesque, and J. Zinn-Justin (North-Holland, Amsterdam, 1991).
[56] W. van Megen and P. N. Pusey, Phys. Rev. A **43**, 5429 (1991).
[57] W. Petry, E. Bartsch, F. Fujara, M. Kiebel, H. Sillescu, and B. Farago, Z. Phys. B: Condens. Matter **83**, 175 (1991).
[58] J. Wuttke, J. Hernandez, G. Li, G. Coddens, H. Z. Cummins, F. Fujara, W. Petry, and H. Sillescu, Phys. Rev. Lett. **72**, 3052 (1994).